LATTICE BOLTZMANN SIMULATION OF FLUID FLOW IN POROUS MEDIA OF TEMPERATURE-AFFECTED GEOMETRY[1]

ARKADIUSZ GRUCELSKI

Institute for Chemical Processing of Coal, Zabrze, Poland and
Institute of Fluid-Flow Machinery, Polish Academy of Sciences, Gdańsk, Poland
e-mail: agrucelski@imp.gda.pl

JACEK POZORSKI

Institute of Fluid-Flow Machinery, Polish Academy of Sciences, Gdańsk, Poland
e-mail: jp@imp.gda.pl

The Lattice Boltzmann method (LBM) has been applied for flow and heat transfer computations. The simulations have been performed with the single-relaxation time model and an advanced formulation of boundary conditions for LBM. For non-isothermal cases, a second distribution function has been used. First, validation tests are reported for heated flow past a single obstacle as well as over a set of regularly and randomly arranged obstacles (grains) that make up a simplified model of a porous medium. The Nusselt number for heat transfer in flow past a single obstacle has been computed. Next, novel simulations of non-isothermal flow in a porous medium of temperature-affected geometry have been undertaken. For the purpose, the thermal dilatation of grains has been accounted for. Results are presented for the pressure head loss and time-varying temperature profiles in the medium. Qualitative computations accomplished to date constitute an encouraging first step to proceed further towards the impact of temperature-affected geometry in such flows, in particular for the coking process.

Key words: Lattice Boltzmann Method, porous media flow and heat transfer, variable geometry

1. Introduction

The coking plants are widely used to provide chemically cleaner coal (coke), coke-oven gas and other products. A detailed analysis of the coking process

---

[1]Presented at the XIX Polish Fluid Mechanics Conference, Poznań, September 5-9, 2010.

has gained a renewed interest nowadays (cf. Nomura and Arima, 2000; Guo and Tang, 2005), since ecological trends impose regulations to build industrial objects with Best Available Technology. Apart from fluid flow and heat transfer, changing shape and volume of coal grains is observed during the process; at the same time, production of the coking gas takes place as a consequence of chemical reactions occurring with growing temperature. The complexity of physico-chemical phenomena and complication of geometry imply that the use of more traditional tools and software of computational fluid dynamics (CFD) becomes prohibitively expensive. Hence the idea of a multiscale approach for detailed simulation purposes. In that approach, a microscopic (single-pore level) computation of the representative element of volume (REV) is followed by a macroscopic CFD (system-level) computation (unsteady 1D/2D).

Numerical simulations of the coking process in the macroscale need, as an input, several closure relationships that will provide variables describing geometrical properties of the domain that change during simulation. Only limited experimental data exist, along with a few examples of CFD investigations, cf. Guo and Tang (2005). We find it useful to provide the necessary input from detailed simulations in the microscale. As a numerical approach at the single-pore level, we have chosen the lattice Boltzmann method (LBM).

The LBM, based on the Boltzmann equation (He and Luo, 1997), has been developed in early 1980s as a method designed originally to be an extension of cellular automaton (Rothman and Zaleski, 1997) for eliminating large numerical noise. The LBM has proven to be suitable for simulations of viscous and nearly incompressible fluid flows (Succi, 2001; Chen and Doolen, 1998) as well as heat transfer (He *et al.*, 1998) in simple (Yu and Girimaji, 2005) and complex geometries (Pan *et al.*, 2006). The present authors have successfully applied the LBM to flow past obstacles and also to thermal problems (Grucelski and Pozorski, 2009, 2011). The phenomenon of changing volume and shape of grains in function of temperature can be dealt with more advanced boundary schemes for LB method. In our approach, the internal energy density distribution function (IEDDF) solves for a temperature field, separately from velocity and pressure fields (Wang *et al.*, 2007); the on-site interpolation-free (OSIF) boundary scheme accounts for the change of grains shape with temperature (Kao and Yang, 1998).

LBM simulations in variable geometry are still under development. Some disadvantage of such calculation is a higher numerical cost caused by application of more complicated boundary schemes. An interesting case of flow simulation with moving boundaries is reported by Krafczyk *et al.* (2001) where authors present LBM results of fluid flow through a heart valve. Yet, we

are unaware of any publication where the heat transfer problem has been implemented for flow modelling in variable geometry.

In the present paper, we build on our experience to date and further develop the LBM approach. We briefly recall the main idea of the method and describe our current implementation of LBM to compute heat transfer coefficients in a flow past a single obstacle. Then, we address the issue of flow and heat transfer in a generic (computer-generated) porous medium and present some results for the pressure loss and temperature fields. The main novel point of the present work is the accounting for variable geometry effects related to displacements of solid-fluid interfaces due to temperature increase in the porous medium.

2.   Lattice Boltzmann Method

2.1.   Governing equations

The numerical tool used in our simulations stands between molecular dynamics (where we track position of every molecule and its velocity, like in simulations of fracture propagation) and computational fluid dynamics (where we concentrate on macroscopic conservation laws, i.e., the Navier-Stokes equations). LBM is based on the Boltzmann equation (Succi, 2001) governing the evolution of density distribution function f that describes the probability density of finding particles with velocity $\boldsymbol{u}$, at some infinitesimal volume with the centre at $\boldsymbol{r}$

$$[\partial_t + \boldsymbol{u} \cdot \boldsymbol{\nabla}_r + \boldsymbol{F} \cdot \boldsymbol{\nabla}_u] f(\boldsymbol{r}, \boldsymbol{u}, t) = \int \sigma(\Delta \boldsymbol{u}_{12}, \Psi)(f_{1'2'} - f_{12}) \, d\Psi \qquad (2.1)$$

where $\sigma = \sigma(\Delta \boldsymbol{u}_{12}, \Psi)$ in the RHS collision term describes the number of particles with relative speed $\Delta \boldsymbol{u}_{12}$ in a solid angle Ψ; symbols f_{12} and $f_{1'2'}$ stand for two-particle distribution functions before and after collision, respectively. The LHS of Eq. (2.1) describes the Newtonian mechanics of a set of molecules; the RHS stands for the interaction term describing the number of particles lost from and coming into an element of the phase space as a result of collisions. The crucial feature of LBM (Rothman and Zaleski, 1997; Succi, 2001) is discretisation of the microscopic velocity vectors, both in direction and magnitude, cf. Fig. 1 for some schemes used in 2D or 3D flows (9 or 15 velocities, respectively). A lot of algebra is needed to discretise the above equation (He and Luo, 1997), also we have to use the H-theorem (Succi, 2001) to simplify its RHS.
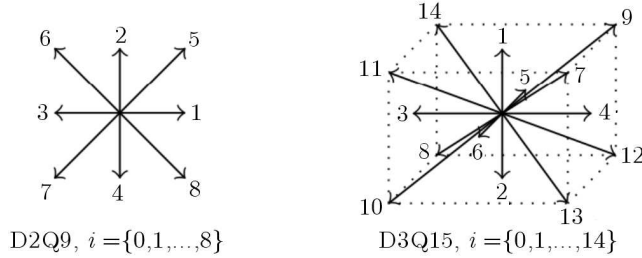
Fig. 1. Examples of LBM discretisation of velocity space in 2D and 3D

Subsequently, the RHS of Eq. (2.1) is modelled by a relaxation term (cf. below). The equation is discretised in time (by the time step δt), in space (by the lattice size δx), and in velocity space by distinction of admissible directions $\boldsymbol{e}_i$ (i subscript, cf. Fig. 1) of the particles velocity on a regular square lattice. After these steps, the Lattice Boltzmann equation (suitably non-dimensionalised with δt as the time scale and δx as the length scale) takes the form (cf. Chen and Doolen, 1998)

$$f_i(\boldsymbol{r} + \boldsymbol{e}_i \delta t, t + \delta t) = f_i(\boldsymbol{r}, t) - \tau_\nu^{-1}(f_i - f_i^{eq}) \tag{2.2}$$

where f_i^{eq} describes the equilibrium state of density $f_i(\boldsymbol{r}, t)$ that for fluid flow problems has the following form

$$f_i^{eq} = \rho \Omega_i \Big[1 + 3\boldsymbol{e}_i\boldsymbol{v} + \frac{9}{2}(\boldsymbol{e}_i\boldsymbol{v})^2 - \frac{3}{2}\boldsymbol{v}^2\Big] \tag{2.3}$$

In Eq. (2.3), ρ and $\boldsymbol{v}$ are the local fluid density and velocity, respectively, the weight coefficients Ω_i depend only on the discretisation model of the velocity space. For two presented sets of lattice velocity discretisation (D2Q9 and D3Q15), the coefficients of velocity expansion are constant. In Eq. (2.2), the relaxation time τ_ν has the following non-dimensional form

$$\tau_\nu = \frac{1}{2} + 3\nu^+ \tag{2.4}$$

In the above equation, $\nu^+ = \nu\delta t/\delta x^2$ is the non-dimensional kinematic viscosity of the fluid.

Historically, two closely related schemes for LBM have been proposed. The first is the single relaxation time (SRT) approach used here, Eq. (2.2), known as Bhatnagar-Gross-Krook (BGK, Bhatnagar *et al.*, 1954), where the microscopic relaxation time is related to the macroscopic variable describing fluid viscosity, Eq. (2.4). Another approach developed by d'Humières *et al.* (2002) uses the

matrix of relaxation times; some additional cost and complexity are balanced by better stability properties and precision.

The single relaxation time (SRT) approximation in the presented form is not appropriate for simulating heat transfer phenomena (He *et al.*, 1998), interesting from the practical point of view. The main reason is constant Prandtl number $Pr = 1$ and occurrence of instabilities in the course of computations. A possibility to overcome these difficulties while dealing with heat transfer problems in the BGK approximations is to extend the formulation with two distribution functions (He *et al.*, 1998), namely the mass density f_i and an additional, internal energy density distribution function (IEDDF) g_i with its own relaxation time. Thus the BGK LBM with an additional equation for solving heat transfer becomes a double relaxation time approach. The scheme appears to be very stable when compared to other work for solving heat transfer problems with LBM (Peng *et al.*, 2003b). Yet, the method reveals to be complex, mainly because of gradient terms in the evolution equation (Wang *et al.*, 2007).

In the present work, we apply a simplified variant of the IEDDF, elaborated by Peng *et al.* (2003b). It is widely used and developed also to implement source terms due, e.g., to chemical reactions (Wang *et al.*, 2007). The thermal lattice Boltzmann equation can be written as

$$g_i(\boldsymbol{r} + \boldsymbol{e}_i\delta t, t + \delta t) = g_i(\boldsymbol{r}, t) - \tau_\theta^{-1}(g_i - g_i^{eq}) \tag{2.5}$$

where g_i^{eq} stands for the internal energy density equilibrium distribution function in $(\boldsymbol{r}, t)$ and has the following form

$$g_i^{eq} = \theta \Omega_i [a_i + b_i \boldsymbol{e}_i \boldsymbol{v} + c_i (\boldsymbol{e}_i \boldsymbol{v})^2 + d_i \boldsymbol{v}^2] \tag{2.6}$$

where Ω_i is the weight coefficient, θ is the local temperature (cf. below); the coefficients a_i through d_i depend on the chosen model of velocity discretisation and also on the direction i, unlike those in Eq. (2.3). A full description of given equations, with exact arrays of coefficients for Eq. (2.6), can be found in Wang *et al.* (2007) for D2Q9 model and Peng *et al.* (2003a) for D3Q15 and D3Q19 models. The thermal relaxation time in phase m has the following form

$$\tau_\theta = \frac{1}{2} + \frac{3}{2} \frac{\lambda_m}{\rho c_{pm}} \frac{\delta t}{\delta x^2} = \frac{1}{2} + \frac{3}{2} \alpha_m^+ \tag{2.7}$$

written both for the fluid f (gases) and solid s (coal grains) in the computational domain, so $m \in \{s, f\}$. The heat diffusivity α_m is expressed in terms of the heat conductivity λ_m and the specific heat c_{pm}. The relaxation times

τ_ν and τ_θ depend on flow parameters (viscosity and thermal diffusivity). We note that both must be chosen within the range where the solution remains stable, for example $\tau_\nu \in (0.5, 2)$.

On the basis of the mesoscopic formulation, we use the following summation expressions (discretised integrals) to obtain local macroscopic flow variables (Wang *et al.*, 2007), i.e., the fluid density, velocity and temperature

$$\rho = \sum_i f_i \qquad \boldsymbol{v} = \frac{1}{\rho} \sum_i f_i \boldsymbol{e}_i \qquad \theta = \sum_i g_i \qquad (2.8)$$

Equations (2.2) and (2.5) with appropriate equilibrium distributions are presented in a non-dimensional form and are valid with the assumption of a low Mach number ($M = v_x/c \ll 1$) where v_x is a flow velocity scale and $c = \delta x/\delta t$ is the lattice sound speed. This assumption is controlled in two ways in the performed computation. First, the maximum flow velocity is checked to be a fraction (less than 10%, say) of the sound speed. Second, the maximum variation of the density field is also checked to be smaller than several percent. Our experience has shown that larger variations in density may lead to numerical instabilities. In that case, computation is repeated on a finer mesh with a shorter time step.

The LBM simulation is divided into three following steps for every lattice node at each time instant. First is a simple propagation of the distribution functions in discrete directions, cf. the LHS of Eqs. (2.2) and (2.5). In the second step we apply boundary conditions and collision (relaxation) terms for density and internal energy distribution functions. In the last step we perform gathering and calculating of macroscopic data from Eqs. (2.8).

2.2. Domain construction

In our first LBM simulations for a single obstacle we considered the case of heat transfer in a hot fluid flow over a cold circular cylinder (cf. Sec. 3.2), originally used to calculate the Strouhal number of unsteady vortex shedding, cf. Grucelski and Pozorski (2009, 2011).

As far as the construction of porous media is concerned, the domain consists of several REVs. A single REV is created by randomization of radii with uniform distribution within the prescribed range (r_{min}, r_{max}); centres of the obstacles are uniformly distributed in the computational area. The diameter of obstacles is much smaller than the domain size. In our simulation, the obstacles can penetrate each other and also intersect the boundary of the domain; the algorithm next will periodically shift them (Fig. 2). In the modelling of

flow and heat transfer in temperature-affected geometry, we start with a regular array of cylinders in a staggered arrangement (with centres located at vertices of equilateral triangles), followed by simulations in a random array of obstacles.
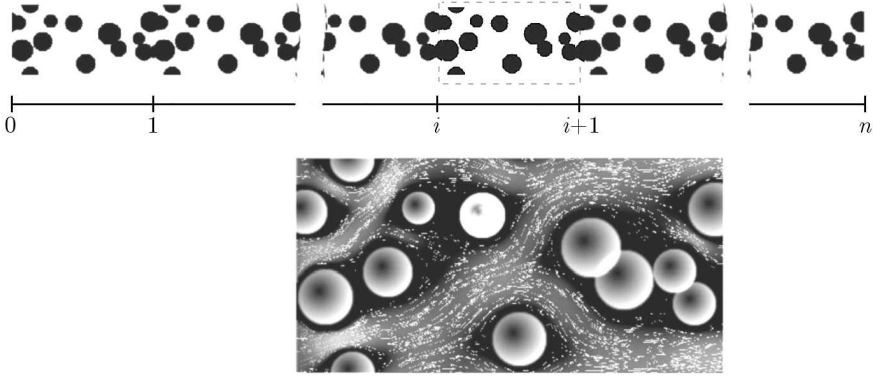
Fig. 2. Construction of a simple porous medium for flow simulation with zoom of a single REV (gray scale represents the fluid velocity magnitude)

In the case of flow in fixed geometry, the obstacles are represented as follows: every LBM node inside the circular cylinder with a given radius is given a "solid" identifier; outside nodes lying close $(0.3\delta x$, say) to the cylinder surface are also identified as solid. Next, every solid node which has at least one neighbouring fluid node is labelled as "interface". For the case of changing shape, the nodes nearest to the real surface of the obstacle are next processed for more complicated boundary schemes.

2.3. Inlet/outlet boundary condtion

The inlet condition is applied by simple calculation of f_i in unknown directions from known distribution functions within the flow domain, the imposed inlet velocity and density. The following relationships are used for appropriate indices $i \in \{0, 1, 2, 4, 5, 8\}$, cf. Fig. 1a

$$f_i^{neq} = f_{-i}^{neq} \qquad \text{or} \qquad f_i = f_{-i} - (f_{-i}^{eq} - f_i^{eq}) \qquad (2.9)$$

where f_{-i} corresponds to the direction $\boldsymbol{e}_{-i} = -\boldsymbol{e}_i$; the non-equilibrium distribution function is defined as $f_i^{neq} = f_i - f_i^{eq}$. The imposed (macroscopic) fluid velocity and density at the flow inlet enter the distribution function f_i^{eq} through Eq. (2.3). In the case of heat transfer computations, we additionally impose the inlet temparature. Again, it is used in the equilibrium distribution of

IEDDF, Eq. (2.6), at the flow inlet. In terms of the distribution function g_i^{neq}, we apply the following equation (cf. Wang *et al.*, 2007)

$$g_i^{neq} - \boldsymbol{e}_i^2 f_i = -g_{-i}^{neq} + \boldsymbol{e}_{-i}^2 f_{-i}$$

with $g_i^{neq} = g_i - g_i^{eq}$.

To implement the boundary condition at the outlet (where neither velocity nor pressure is imposed), we use the extrapolation of known distribution functions for $i \in \{3, 6, 7\}$

$$f_i(\boldsymbol{r}, t) = \frac{1}{2}[f_i(\boldsymbol{r} - e_{-i}\delta t, t) + f_i(\boldsymbol{r} - 2e_{-i}\delta t, t)] \qquad (2.10)$$

To fix the Reynolds number as a given parameter in the flow cases considered, we set the inlet velocity v_x, $\boldsymbol{v} = [v_x, 0]$. Then, $\mathrm{Re} = d^+ v_x^+ / \nu^+$ where d^+ is the number of lattice nodes per typical obstacle diameter.

2.4. Wall boundary schemes in LBM

For flow and heat transfer simulations we apply periodic conditions on the longer side of the domain (parallel to the main flow direction), cf. Fig. 5. At the inlet we impose a uniform velocity profile on every fluid node with constant density and temperature. For the outlet nodes we use the extrapolation condition, based on nodes inside the domain.

For fluid flow past fixed geometry we use the non-equilibrium (NEq) bounce-back scheme for boundary conditions at the solid-fluid interface. The scheme shows second-order accuracy and better stability than the original bounce-back scheme (Zou and He, 1997), acceptable implementation complexity and computational cost, with the following condition for unknown values of distribution function

$$\boldsymbol{x} + \boldsymbol{e}_i \delta t = \mathcal{S} \quad \Rightarrow \quad f_{-i}^{neq}(\boldsymbol{x}, t + 2\delta t) = f_i^{neq}(\boldsymbol{x}, t) \qquad (2.11)$$

where $\mathcal{S}$ stands for a solid node. These boundary conditions are a developed form of the no-slip bounce-back method (Derksen, 2006) and show good accordance with results obtained with more advanced boundary schemes (Grucelski and Pozorski, 2011).

Basically, phenomena of flow in variable geometry cannot be simulated in LBM with the NEq method; for such computations, instabilities occur after changing the identifier of a single node (closer than $0.1\delta x$ from the interface, say) from fluid to solid one. To simulate phenomena of the shape change in function of growing temperature, we have to implement a more complex

boundary condition, allowing for reconstruction of the real interface. One of such methods is the on-site interpolation-free scheme (OSIF), described in details by Kao and Yang (1998). Aside of possibility of simulating moving boundaries, this method is free from interpolation that may cause a non-zero mass flux through the solid-fluid interface.

The OSIF scheme is based on weighting the relaxation time at nodes near the interface. As shown in Fig. 3, we define the weight coefficient q $(0 < q \leqslant 1)$

$$q = \frac{|\boldsymbol{r}_f - \boldsymbol{r}_s|}{\delta x} \qquad (2.12)$$

where $\boldsymbol{r}_s$ and $\boldsymbol{r}_f$ describe the positions of the solid node and real interface of the obstacle, respectively. The weighted (body-fitted) relaxation time $\tau^{(bf)}$ is introduced as

$$\frac{1}{\tau^{(bf)}} = \frac{2q}{q - 1 + 2\tau^{(mf)}} \qquad (2.13)$$

where the mesh-fitted relaxation time $\tau^{(mf)}$ is equal to τ_ν.
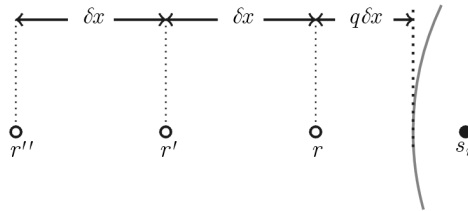
Fig. 3. A sketch of the weight coefficient q for the OSIF boundary scheme

With known relaxation time, we calculate the distribution function $f_i^{(bf)}(\boldsymbol{r}, t)$ in the direction into a solid node (using the discrete set of directions, cf. Fig. 1) from the formula

$$f_i^{(bf)} = f_i^{eq} + [f_i^{(mf)} - f_i^{eq}]q\frac{\tau^{(bf)} - 1}{\tau^{(mf)} - 1} \qquad (2.14)$$

The OSIF simulation has the following algorithm. First, the weighted distribution function $f_i^{(bf)}$ is calculated with Eq. (2.14) in a chosen direction. Next, the distribution function is moved (advection) into an interface node. According to the bounce-back scheme, we revert the distribution function on interface nodes at the third step (collision). The distribution is next moved into a fluid node (advection). For a full description of the OSIF scheme, see Grucelski and Pozorski (2011).

For the present computations, we still applied the non-equilibrium bounce-back boundary condition for g_i at the solid-fluid interface (mainly for the

sake of simplicity at the time being), cf. Peng *et al.* (2003). The unmodified condition can be rewritten

$$g_i^{neq} - \boldsymbol{e}_i^2 f_i^{neq} = -g_{-i}^{neq} + \boldsymbol{e}_{-i}^2 f_{-i}^{neq} \tag{2.15}$$

3. Results for validation cases

3.1. Fluid flow

The LBM approach described above was validated in a few tests for fluid flow phenomena in simulated porous media. We checked the results against the macroscopic, empirical laws for porous media flows: the Darcy law for low inlet velocity, and the extended formula, with the additional Forchheimer term (Vafai and Amiri, 1998), for higher inlet velocity

$$\nabla \langle p \rangle = -\frac{\varepsilon \nu}{K} \langle \boldsymbol{u} \rangle - \varepsilon^2 \rho \beta |\langle \boldsymbol{u} \rangle| \langle \boldsymbol{u} \rangle \tag{3.1}$$

where $\langle \cdot \rangle$ stands for volume averaging, $\varepsilon = V_f/V$ is porosity, K is permeability (the first-order term describing viscous resistance) and β is the Forchheimer coefficient (the second-order term describing inertial effects in porous media flow).

The above-mentioned law is described in detail in Scheidegger (1957) with an exhaustive discussion of the permeability coefficient. It is well known that the Darcy equation was first obtained as an empirical law. As it is presented by Vafai and Amiri (1998), the law describing flow over porous media in the macroscale could be retrieved with usage of the Navier-Stokes equations averaged over fluid volume

$$\rho(\partial_t \langle \boldsymbol{u} \rangle + \langle \boldsymbol{u} \rangle \cdot \nabla \langle \boldsymbol{u} \rangle) = -\nabla \langle p \rangle + \mathcal{D} + \mathcal{F} \tag{3.2}$$

$\mathcal{D} = -\varepsilon \nu \langle \boldsymbol{u} \rangle / K$ is known as the Darcy term (viscous effects); $\mathcal{F} = -\varepsilon^2 \rho \beta |\langle \boldsymbol{u} \rangle| \langle \boldsymbol{u} \rangle$ is known as the Forchheimer term (inertial effects) with β depending only on geometrical properties of a domain. The Brinkman term (Kim and Ghiaasian, 2009) is omitted from Eq. (3.2) for simplicity. The coefficients K and β have a complex integral form (cf. Kim and Ghiaasian, 2009) over a surface of grains in the domain. It is possible to obtain the permeability in an analytical way only for very simple cases as flow over a regular array of spheres with constant radius. In the case of more complex geometries, we obtain both coefficients from the LBM simulations at the single grain level.

Simulations of this kind are hard to manage, especially for geometry varying with time.

Figure 4 shows a comparison of the average pressure loss per single REV (symbols) with the Darcy-Forchheimer law, Eq. (3.1), and the Darcy law. The
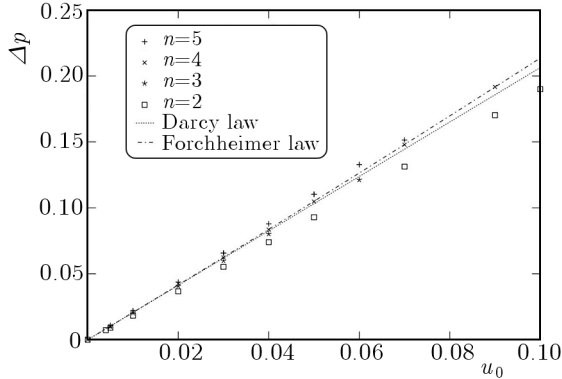
Fig. 4. The average pressure loss vs. the inlet velocity for a few lengths of the numerical domain (n periodically copied REVs). The symbols denote LBM results, lines – empirical laws

pressure losses are obtained from the LBM flow simulations for a selection of bulk velocity values in the medium: $u_0 = \langle v_x \rangle$. First, the permeability coefficient (describing viscous resistance of domain geometry) is obtained for low inlet velocities from the Darcy equation: $K = -\varepsilon \nu \langle v_x \rangle / \nabla \langle p \rangle$ where $\nabla \langle p \rangle$ is taken from simulation points. The results have been gathered for a few lengths of the computational domain that consisted of n periodically copied REVs. Next, we obtained the quadratic coefficient β (describing inertial resistance of the porous domain) for Eq. (3.1) by the least-square fit to the LBM results. Influence of β coefficient can be observed as a small difference between the Darcy and Darcy-Forchheimer curves describing the pressure loss. The flow computations in random porous media are performed with fairly low Reynolds numbers; for growing Re, simulations start to loose stability (too high local velocity between pores). For such flows, a finer grid has to be used instead. Yet, flow simulations at higher Reynolds numbers (Re > 20) are still possible in regular porous media where local magnitude of velocity is much smaller than the lattice speed of sound.

With usage of the bounce-back scheme for single-relaxation-time (SRT) variant of LBM, it is known that the permeability shows some dependence on viscosity, more important than for the multiple relaxation time (MRT) variant (Pan *et al.*, 2006). We want to point out that Pan *et al.* (2006) compare the simple bounce-back scheme with a few schemes for SRT LBM. More work is

still needed in matter of testing other boundary conditions for SRT LBM, also for the NEq and OSIF schemes used here for both fixed and temperature-dependent geometry.

3.2. Heat transfer

To validate the LBM for non-isothermal flows, we considered the classical problem of cooled flow past a single obstacle, cf. Fig. 5. The Nusselt number, $\mathrm{Nu} = \mathrm{Nu}(\mathrm{Re}, \mathrm{Pr})$, was determined for a couple of Re and $\mathrm{Pr} = \nu/\alpha$. The local and global Nusselt numbers are obtained from

$$\mathrm{Nu}(\phi) = \frac{d}{\theta_w(\phi) - \theta_{in}} \left. \frac{\partial \theta}{\partial n} \right|_\phi \qquad \mathrm{Nu} = \frac{1}{2\pi} \int\limits_\phi \mathrm{Nu}(\phi) \, d\phi$$

where $\boldsymbol{n}$ is the unit vector normal to the solid-fluid interface, d is the cylinder diameter, θ_w is the wall temperature, θ_{in} is the flow inlet temperature, and ϕ is the polar angle measured w.r.t. to the inflow direction. The integral is calculated over the solid-fluid interface.
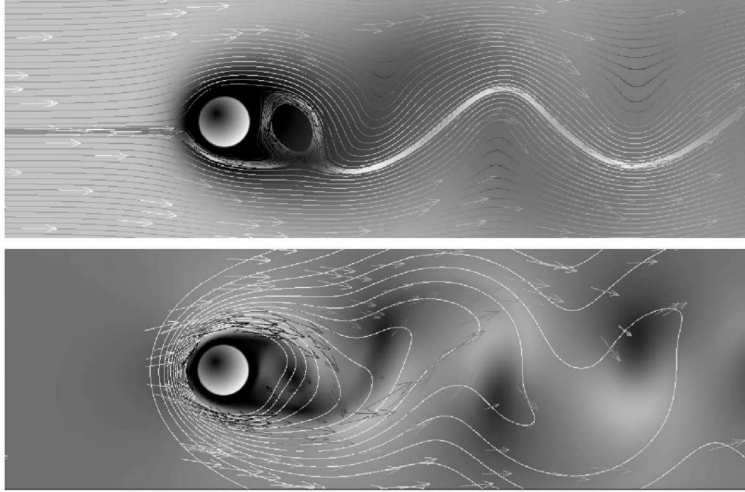
Fig. 5. An example of flow past a circular cylinder at $\mathrm{Re} = 150$; (a) stream lines with velocity vectors and the temperature field coded with a scale of gray; (b) isolines of temperature (also with flow velocity vectors) superposed on the grayscale map of velocity magnitude

The angular distribution of the Nusselt number $\mathrm{Nu}(\phi)$ for a single obstacle is presented in Fig. 6. Because of coarse and square mesh (not a body-fitted one), the observed values of Nu show unphysical, local oscillations. They are

caused by the stair-shape character of the interface. In the next step, the collected values are averaged (typically, over $\delta = \pi/9$) to obtain a smoother result according to

$$\overline{\mathrm{Nu}}(\phi_o) = \frac{1}{2\delta} \int\limits_{\phi_o-\delta}^{\phi_o+\delta} \mathrm{Nu}(\phi) \, d\phi \tag{3.3}$$

For such averaged values we calculate best-fitted, low-level polynomials, cf. Fig. 6. There, the LBM results with the OSIF boundary scheme are obtained on the 500×250 lattice and compared with those reported by Jie and Huiming (2006). In the approximating polynomial we omit the first-order term because of the symmetry constraints: $\partial_\phi \overline{\mathrm{Nu}}(\phi)|_{\phi=0,\pi} = 0$ (i.e., at the upstream and downstream stagnation points). The resulting distributions (points from LBM simulation) still show some variation, not present in the results of Jie and Huiming (2006). Those authors solved the flow with the LBM, and a more traditional CFD approach was used to solve the energy equation on the O-type body-fitted grid what greatly improved smoothness of their results. From the present simulation, the best-fitted curve is in a qualitative agreement with the one reported by Jie and Huiming. For a quantitative comparison, the experimental data of Acrivos *et al.* (1965) have been added in Fig. 6. The present results seem to be quite satisfactory.
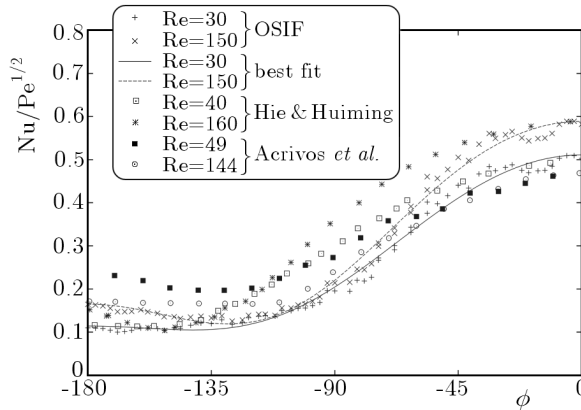
Fig. 6. Local Nusselt numbers Nu in function of the polar angle ϕ for a few Re. Lines represent the best nonlinear fit to LBM simulation points:
$$\mathrm{Nu}(\phi) = a_0 + a_1 \cos\phi + a_2 \cos^2\phi$$

We want to point here that the OSIF scheme assumes weighting of the mass density distribution function only, while the IEDDF still sees a stair-shaped solid-fluid interface. An improved boundary scheme for non-isothermal

flows remains an open issue. This brings us to conclude that for a simple rectangular lattice used in the present paper, the curve fitting (smoothing) is necessary. With growing Re we observe that local Nu grow for angles close to the downstream separation point $(\phi = \pi)$ because of vortex shedding. To the best knowledge of the authors, the results for angular distribution of the Nusselt number, where heat transfer is solved by the LBM, are reported for the first time here.

In LBM computation, we first simulate isothermal fluid flow at the inlet temperature θ_{in} past the obstacle (initially, of temperature θ_o). When the vortex shedding becomes regular, the global Nusselt number has been calculated (Grucelski and Pozorski, 2009). The obtained values are presented in Fig. 7. As we can see, the results show good conformity with empirical laws, like for example Daloglu and Unal (2000). Here, for approximation (lines) we use the relationship for the Nusselt number basing on the Ranz-Marshall correlation $Nu = 2 + 0.572Re^{0.5}Pr^{0.3}$, where we fit its coefficients. For flow past a circular cylinder another empirical correlation is $Nu = 0.3609Re^{0.5749}$, cf. Daloglu and Unal (2000). In the case of $Re \to 0$, for which LBM simulations loose stability, we add the point $Nu(Re = 0, Pr) = 2$.
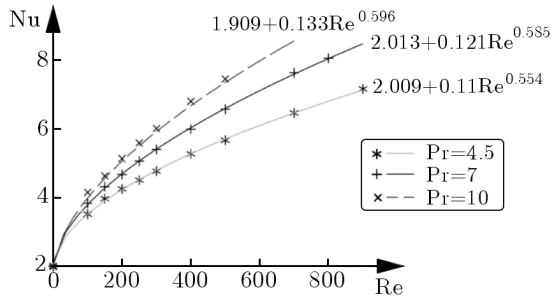
Fig. 7. Global Nusselt number Nu as a function of Re for a few Pr numbers.
Solid lines represent the best nonlinear fit to simulation points
with $Nu = a + bRe^c Pr^d$

Then, we have performed LBM simulations of convective heat transfer in a porous medium of fixed geometry. Figure 8 illustrates the heating of the medium. The temperature evolution in two selected cross-sections is shown in Fig. 9. Currently, work is underway to retrieve a macroscopic law describing heat transfer in the porous medium.
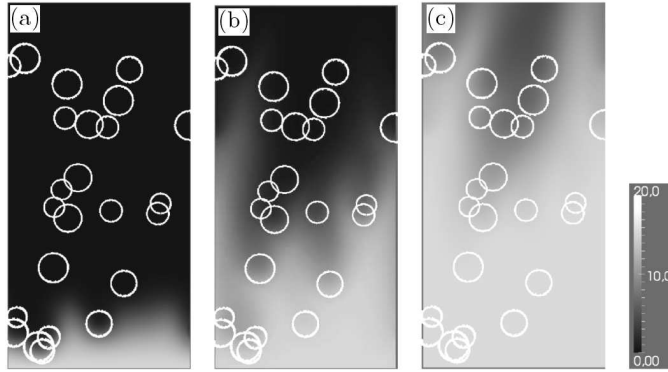
Fig. 8. Evolution of the temperature field in a computer-created porous medium (the main flow direction is upwards). White circles represent the boundary of the obstacles; (a) $tv_x/d = 0.45$, (b) $tv_x/d = 2.25$, (c) $tv_x/d = 5.25$
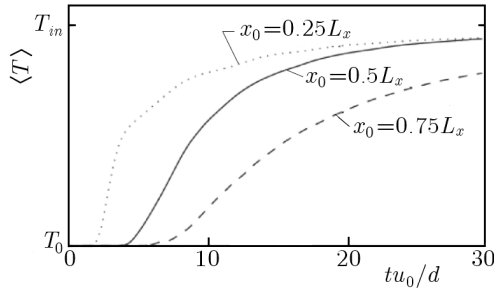
Fig. 9. Averaged temperature profile over lattice nodes at different downstream stations of REV

4.   Variable geometry

As mentioned in the Introduction, an essential part of the coking process is the thermal expansion and plastic deformation of coal grains. Therefore, we develop LBM simulations for the case of temperature-affected geometry of the porous medium. Here we assume that there is a maximum radius of each obstacle, and we simplify the model by imposing no mechanical interactions of the fluid-solid and solid-solid type (growing grains would overlap each other eventually).

For simulation of variable geometry with the NEq scheme, one will encounter stability problems that may occur even for a change of only a few fluid nodes into solid ones. With the OSIF scheme, simulations of flow in temperature-affected geometry remain stable. In the case of overlapping inter-

faces of the obstacles, one will be faced with stability issues connected with the thin layer (of one node width) of the fluid. To cope with those problems, in the case where there are two obstacles with interfaces in distance of a single lattice step, for the fluid node we choose the obstacle whose interface is closer; for that particular value of q, cf. Eq. (2.12), we weight every distribution function pointing at the obstacle interface.
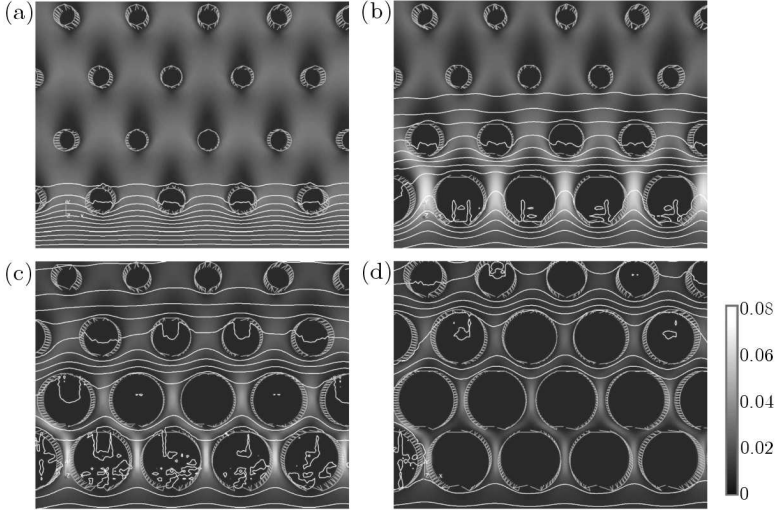
Fig. 10. LBM simulations of the volume change with growing temperature of obstacles in regular geometry; four time instants. Lines represent constant temperature and gray-scale map codes the magnitude of velocity (the main flow direction is upwards); (a) $t = 500$, (b) $t = 1500$, (c) $t = 3000$, (d) $t = 4500$

First, we considered a regular arrangement of N obstacles (cylinders) with a finite thermal conductivity and a temperature-dependent size, according to

$$d_n(t) = d_o[1 + \beta(\theta_n(t) - \theta_o)] \qquad (4.1)$$

where θ_o is the initial temperature of the set of obstacles (simulated porous medium) and $d_n(t)$, $\theta_n(t)$ are the (time-varying) diameter and average temperature of obstacle n $(n = 1, \ldots, N)$, respectively. Figure 10 shows first simulations with changing size of the obstacles (temperature-affected geometry). Analogously to results discussed in Secs. 2 and 3, we have computed some integral characteristics of a simulated, variable-geometry porous medium. Figures 11 and 12 show the time evolution of porosity, the total pressure loss in the system and its average temperature, respectively. The two simulation variants are compared: fixed geometry and changing size of the obstacle according to Eq. (4.1). It is seen that, with the increasing temperature, the pressure

loss exhibits a rapid growth, mainly due to the first upstream row of obstacles (already heated) that expand. Consequently, the viscous resistance will considerably increase. During flow evolution, where the porosity asymptotically attains a constant value, we also perceive much smaller change of pressure loss than the one observed at the start of flow. Time records of the averaged temperature profile are also different from those observed for flow past a fixed geometry. Figure 12 seems to agree with intuition that for flow with a larger pressure loss, the heat transfer through the array of obstacles is much slower, due to a smaller mass flow rate. This also causes the fluid to cool down faster.
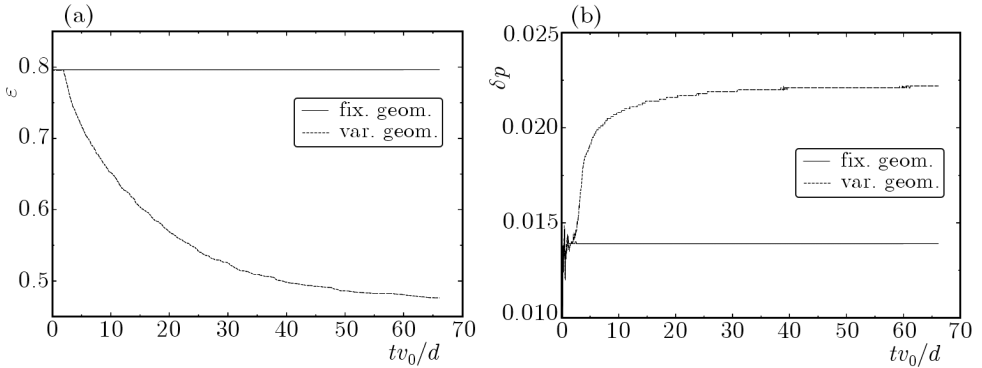
Fig. 11. Time evolution of: (a) porosity and (b) pressure difference between the inlet and outlet for flow through computer-created, variable porous media compared with results for flow in fixed geometry
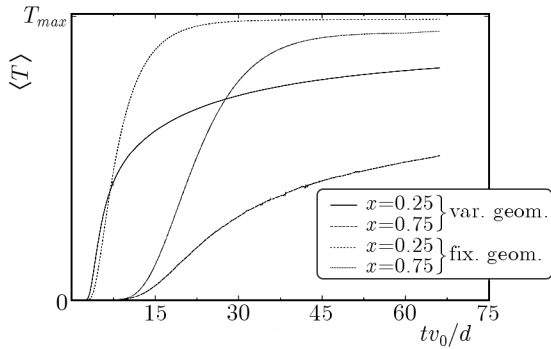
Fig. 12. Time record of the averaged (over fluid and solid nodes) temperature profile at two different downstream stations of the porous medium. Results for flow in variable geometry are compared with results for fixed geometry

Next achievement for the variable-geometry case is an implementation of LBM for a simulation with obstacles that can cross each others interface. For

the time being, however, we do not consider a true mechanical interaction of individual obstacles. Solution of the thermal deformation (which represents a problem in itself) is left for a subsequent work, along with the implementation of plastic interactions between obstacles and next (if reasonable) fluid-structure interaction.

An example of such a simulation is presented in Fig. 13. There, plots (a) show a part of the domain where cold fluid flow is present (the gray maps represent the velocity magnitude and temperature). Plots (b) present the same flow region (partially with changed geometry) with a partially heated fluid. In plots (c), we observe stopping of flow due to overlapping of growing obstacles. We note that shortly before the flow becomes blocked due to neighbouring obstacles getting close to each other, the local fluid velocity in a narrow gap between them can become quite high, occasionally causing numerical stability problems.
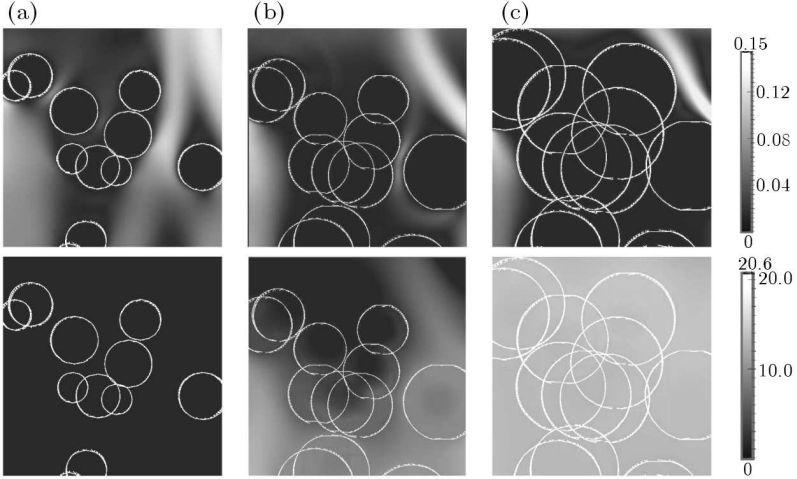
Fig. 13. LBM simulations of volume change with growing temperature and intersections of obstacles in random arrangement. Upper plots: color-coded flow velocity magnitude (upwards mean flow); lower plots: temperature map; (a) $t = 2000$, (b) $t = 10000$, (c) $t = 18000$

5. Discussion and conclusions

In the present work, we have developed LBM into simulation of fluid flow and heat transfer in porous media to retrieve macroscopic variables describing both phenomena at the REV level. We have shown a comparison of the results from

simulation of fluid flow and heat transfer with empirical laws. The pressure loss in function of the inlet velocity allows us to calculate the permeability from LBM simulation data. The permeability obtained in that way shows good conformity with the Darcy-Forchheimer law where the second-order coefficient has been fitted to data points. As we show, the pressure loss on a single REV for different lengths of a domain may vary, but can still be described by the Darcy equation. Using the Forchheimer term (for the inertial effects occurring in faster flow past a porous medium) we can describe the change of pressure loss also for faster (less viscous) flows. During our work, also a change of the permeability with Re was observed. A wider discussion can be found elsewhere (Pan *et al.*, 2006; Grucelski and Pozorski, 2011).

Heat transfer in flow over a single obstacle has been checked also by comparison with empirical laws. Local values of $Nu(\phi)$ show some oscillations due to a coarse interface, occurring in the heat transfer problem for both body-fitted (OSIF) and mesh-fitted (NEq) schemes. Yet, the best-fit polynomials show a good agreement with the experimental data; also, they have been compared to other results connected with LB method (Jie and Huiming, 2006). Global Nusselt numbers for such a flow can also be well correlated by the best-fit curves of the presumed type. Still more work is needed to obtain a better agreement of this type of results, as the local Nusselt numbers, with other numerical schemes (reference data are available).

Because Eq. (2.2) does not have any source term, the distribution function does not depend on temperature. (Later we are going to add sources due to chemical reactions.) Consequently, the applied model is not yet ready to simulate the coking process. At the moment, we can compute heat and fluid flow phenomena in temperature-affected, complicated geometry (of regular or random placement of obstacles). The presented results (change of pressure loss with changing porosity) are consistent with the physical expectation about flow past a porous media; basing on the mentioned results, we also conclude that the changes of averaged temperature for fixed and variable geometry are qualitatively correct. Still, there is a need for quantitative results from LBM simulations of flow and heat transfer phenomena in variable geometry.

Next, we plan to focus on two subsequent developments. First is an appropriate treatment of the situation where the topology changes due to, e.g., nearby solid grains coming in contact (solid-solid interaction). Secondly, we intend to implement the OSIF boundary scheme for the heat transfer problem. As the ultimate objective, we intend to develop an efficient and accurate method to model the coking of coal. We will use the obtained coefficients as closures in a physically-sound, one-dimensional simulation of the process.

References

1. ACRIVOS A., SNOWDEN D.D., GROVE A.S., PETERSEN E.E., 1965, The steady separated flow past a circular cylinder at large Reynolds numbers, *J. Fluid. Mech.*, **21**, 737-760

2. BHATNAGAR P.L., GROSS E.P., KROOK M., 1954, A model for collision processes in gases. I. Small amplitude processes in charged and neutral one-component systems, *Phys. Rev. A*, **94**, 511

3. CHEN S., DOOLEN G.D., 1998, Lattice Boltzmann method for fluid flows, *Annu. Rev. Fluid Mech.*, **30**, 329-364

4. GRUCELSKI A., POZORSKI J., 2009, Lattice Boltzmann simulation of flow and heat transfer in porous media, *Conference on Computational Methods for Thermal Problems*, Naples, Italy

5. GRUCELSKI A., POZORSKI J., 2011, Lattice Boltzmann simulations of flow past an obstacle and in simple porous media, submitted to *Computers and Fluids*

6. DALOGLU A., UNAL A., 2000, Heat transfer from a cylinder in the wake flow, *Int. Comm. Heat Mass Transfer*, **27**, 569-580

7. DERKSEN J.J., 2006, The lattice Boltzmann method for (multiphase) fluid flow simulations, *Lecture Notes, CISM School*, Udine

8. D'HUMIÈRES D., GINZBURG I., KRAFCZYK M., LALLEMAND P., LUO L., 2002, Multiple-relaxation-time lattice Boltzmann models in three dimensions, *Phil. Trans. R. Soc. Lond. A*, **360**, 437-451

9. GUO Z., TANG H., 2005, Numerical simulation for a process analysis of a coke oven, *China Particuology*, **3**, 373-378

10. HE X., CHEN S., DOOLEN G.D., 1998, A novel thermal model for the Lattice Boltzmann Method in incompressible limit, *J. Comput. Phys.*, **146**, 282-300

11. HE X., LUO L.S., 1997, Theory of the lattice Boltzmann method: From the Boltzmann equation to the lattice Boltzmann equation, *Phys. Rev. E*, **56**, 6811-6817

12. Jie W., Huiming Z., 2006, Laminar flow and heat transfer from a circular cylinder in cross-flow using the Lattice-Boltzmann method, Term Paper, National University of Singapore

13. Kao P.H., Yang R.J., 1998, An investigation into curved and moving boundary treatments in the lattice Boltzmann method, *Annu. Rev. Fluid Mech.*, **146**, 282-300

14. Kim S.M., Ghiaasian S.M., 2009, Numerical modeling of laminar pulsating flow in porous media, *J. Fluids Engng.*, **131**, 141203-9

15. Krafczyk M., Tolke J., Rank E., Schulz M., 2001, Two-dimensional simulation of fluid-structure interaction using lattice-Boltzmann methods, *Comput. Struct.*, **79**, 2031-2037

16. Nomura S., Arima T., 2000, Coke shrinkage and coking pressure during carbonization in a coke oven, *Fuel*, **79**, 1603-1610

17. Pan C., Luo L.S., Miller C.T., 2006, An evaluation of lattice Boltzmann schemes for porous media flow simulation, *Comput. Fluids*, **35**, 898-909

18. Peng Y., Shu C., Chew Y.T., 2003, A 3D incompressible thermal lattice Boltzmann model and its application to simulate natural convection in a cubic cavity, *J. Comput. Phys.*, **193**, 260-274

19. Peng Y., Shu C., Chew Y.T., 2003, Simplified thermal lattice Boltzmann model for incompressible thermal flows, *Phys. Rev. E*, **68**, 026701

20. Rothman D.H., Zaleski S., 1997, *Lattice-Gas Cellular Automata*, Cambridge University Press

21. Scheidegger A.E., 1957, *The Physics of Flow Through Porous Media*, University of Toronto Press

22. Succi S., 2001, *The Lattice Boltzmann Method for Fluid Dynamics and Beyond*, Clarendon Press, Oxford

23. Vafai K., Amiri A., 1998, Non-Darcian effects in confined forced convective flows, *Transport Phenomena in Porous Media*, **1**, 313-329

24. Wang J., Wang M., Li Z., 2007, A lattice Boltzmann algorithm for fluid-solid conjugate heat transfer, *Int. J. Therm. Sci.*, **46**, 228-234

25. Yu H., Girimaji S.S., 2005, Near-field turbulent simulations of rectangular jets using lattice Boltzmann method, *Phys. Fluids*, **17**, 125106

26. Zou Q., He X., 1997, On pressure and velocity boundary conditions for the lattice Boltzmann BGK model, *Phys. Fluids*, **9**, 1591-1598

Symulacje przepływu metodą siatkową Boltzmanna w ośrodku porowatym o geometrii zależnej od temperatury

Streszczenie

Metoda siatkowa Boltzmanna (LBM) została zastosowana do obliczeń przepływu i wymiany ciepła. Symulacje zostały przeprowadzone dla modelu z pojedynczym czasem relaksacji oraz zaawansowanego schematu warunków brzegowych metody LB. Dla przepływów nieizotermicznych, użyto dwóch funkcji rozkładu. Przedstawiono obliczenia testowe nieizotermicznego opływu pojedynczej przeszkody, jak również opływu regularnie oraz losowo rozmieszczonych przeszkód (ziaren), które tworzą uproszczony model ośrodka porowatego. Wyznaczono liczbę Nusselta dla przepływu ciepła w opływie pojedynczej przeszkody. Podjęto symulacje połączonych zjawisk (przepływ i wymiana ciepła) dla ośrodka porowatego o zmiennej geometrii przeszkód. W tym przypadku uwzględniono rozszerzalność termiczną ziaren. Zaprezentowano wyniki dla straty ciśnienia oraz zmienne w czasie profile temperatury dla przepływu przez ośrodek. Uzyskane dotąd jakościowe wyniki stanowią pierwszy krok do dalszych badań wpływu zależnej od temperatury geometrii ziaren ośrodka na przebieg takich przepływów, a w szczególności na proces koksowania.